Recent Polarimetric SAR Models for Danube Delta Monitoring using PALSAR Images

Felix Totir, Gabriel Vasile, Lionel Bombrun, Stefan Constantinescu, Angela Ionita, Florin Serban, Dan Raducanu

RECENT POLARIMETRIC SAR MODELS FOR DANUBE DELTA MONITORING USING PALSAR IMAGES

Felix-Costinel TOTIR[1,2], Gabriel VASILE[1], Lionel BOMBRUN[3], Ştefan CONSTANTINESCU[4], Angela IONIȚĂ[5], Florin ŞERBAN[2], Dan RĂDUCANU[6]

[1]GIPSA-lab, CNRS, Grenoble-INP, 961 rue de la Houille Blanche, BP 46, F - 38402 GRENOBLE Cedex, FRANCE, Email: {felix.totir, gabriel.vasile}@gipsa-lab.grenoble-inp.fr
[2]Advanced Studies and Research Center, 19 In Luca Caragiale street, 020042 Bucharest, ROMANIA, Email: florin.serban@asrc.ro
[3] Laboratoire de l'Intégration du Matériau au Système, 351 Cours de la Libération, 33405 Talence cedex, FRANCE, Email: lionel.bombrun@ims-bordeaux.fr
[4] Department of Geography, University of Bucharest, N. Bălcescu No. 1, Bucharest, ROMANIA, Email: stefanc@geo.unibuc.ro
[5] Research Institute for Artificial Intelligence of Romanian Academy, 13 Calea 13 septembrie, sect. 5, 050711 Bucharest, ROMANIA, Email: aionita@racai.ro
[6] GeoInt, Military Technical Academy, 81-83 Bd. George Cosbuc, sect. 5, 050141 Bucharest, ROMANIA, Email: dan.raducanu@gmail.com

ABSTRACT

A young region, in full process of consolidation and continuously expanding, with ever-changing landscapes, with an inherent complexity, the Danube Delta is a very challenging target for monitoring. The complexity of the site provides an almost ideal environment for testing and evaluating the newest algorithms developed for analyzing and interpreting polarimetric SAR images. The analyzed data consists of PolSAR images acquired at L band by the ALOS / PALSAR system. Firstly, the cross-polarization channels HV and VH are analyzed over wetlands. Secondly, several information extraction, processing and interpretation algorithms are applied: parametric stochastic modeling (SIRV heterogeneous clutter models [1]), hierarchical segmentation, various decompositions (TSVM), etc. The obtained results are consistently compared against ground-truth and both model validation and conclusions are drawn.

1. INTRODUCTION

The Danube Delta is the second largest river delta in Europe and the best preserved on the continent. Largely a biosphere reservation (since 1938 in Romania), the Danube Delta represents a favorable place for the development of highly diverse flora and fauna, unique in Europe. Among these, the Letea subtropical forest was internationally recognized as a biosphere reserve under UNESCO's Man and the Biosphere Program in 1992. The Danube Delta is a low alluvial plain, mostly covered by wetlands and water. The average altitude is 0.52 m ASL, with 20% of the territory below sea level, and more than half not exceeding one meter in altitude.

A young region, in full process of consolidation and continuously expanding, with ever-changing landscapes, with an inherent complexity, the Danube Delta is a very challenging target for monitoring. Both difficult access and the special status of biosphere reserve of the region ask for non-intrusive monitoring methods. Vegetation cover and almost continuous clouding over the region make optical surveillance a difficult task. Radar or, more precisely, SAR (Synthetic Aperture Radar) observation is the natural alternative. The complexity of the site provides an almost ideal environment for testing and evaluating the newest algorithms developed for analyzing and interpreting polarimetric SAR images.

2. PRELIMINARY ANALYSIS OF DATA

The analyzed fully-polarimetric (quad-pol) PolSAR image is acquired at L band by the ALOS / PALSAR system [2] (Level 1.1, JAXA-CEOS format) over the Danube Delta region and has a height (along-track) of 18432 pixels and a width (cross-track) of 1248 pixels.

A multi-look averaging (12 looks) has been considered along-track, in order to both reduce the size of the image and to equilibrate the spatial along-track and cross-track spatial resolutions (the along-track resolution seems much finer in the original image). This procedure does not introduce bias in the following results, since it is similar to analyzing a lower resolution image. In compensation, this averaging reduces the speckle noise.

The obtained image has a height (along-track) of 1536 pixels.

Although the reciprocity of the monostatic radar-target system is assumed, in practice this not copes very well. The two cross-polarization channels had been found to be different. Fig. 1 gives a coarse representation of this difference. Note the relative level of the differences between the two channels and the values of the channels.

The phase difference between the channels S_{12} and S_{21} also shows that for large areas, the two channels differ in both phase and amplitude is also sometimes

important, notably in the water-like regions. One explanation for this behaviour may be advanced in the framework of successive acquisition of S_{12} and S_{21} for rapidly-changing environment (waves), leading to fast temporal decorrelation.

The difference between S_{12} and S_{21} channels is somewhat unexpected, since the reciprocity theorem would have ensured that both channels would return the same signal.

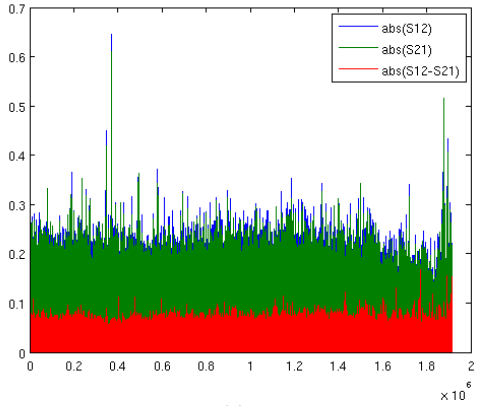

(a)

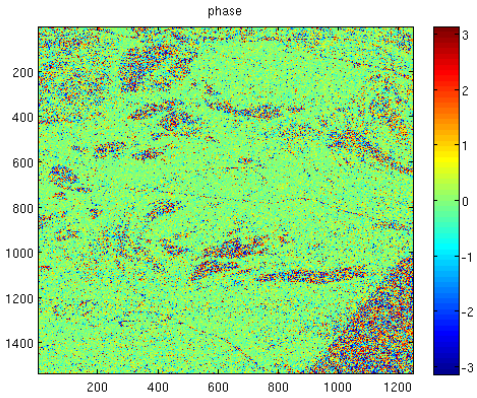

(b)

Figure 1: (a) Comparison of raw S_{12} and S_{21} data and (b) phase difference between S_{12} and S_{21} channels

However, this non-reciprocity condition has been ignored further and the cross-polarization channels has been replaced with their mean ($S_{hv} = (S_{12} + S_{21})/2$). This ensures the reciprocity condition.

3. BASIC POLARIMETRIC DECOMPOSITIONS

3.1. Lexicografic decomposition

The first encoding is the lexicografic decomposition, shown in Fig. 2.

This decomposition makes the following associations between the R, G, B channels of the color image and the polarimetric channels:

- $R = 10\log_{10}\left(|k_{11}|^2\right)$, where $k_{11} = S_{11}$;
- $G = 10\log_{10}\left(|k_{12}|^2\right)$, where $k_{12} = (S_{12} + S_{21})/2$;
- $B = 10\log_{10}\left(|k_{13}|^2\right)$, where $k_{13} = S_{22}$;

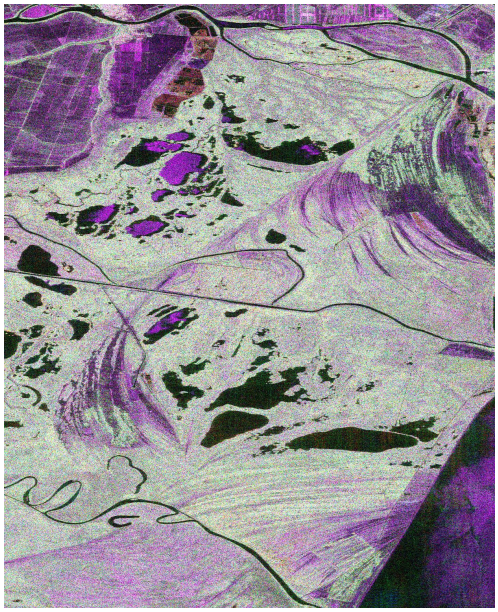

Figure 2: RGB coding of lexicographic decomposition

The lexicografic decomposition completely ignores the relative phases of the polarimetric channels and it is of limited use. However, the green color may indicate the presence of vegetation (notably forest or assimilated), since this component introduces significant depolarization.

Thus, one is able to make the following points:

- still water is signaled by black – for example the Danube channels, the various lakes and the sea next to the shore line;
- purple color may also signal wavy water (open sea), but also particular areas where both channels have similar amplitudes (such like urban areas or rough land);
- green color indicates mainly vegetation, and this is quite predominant in the central region of the image.

3.2. Pauli decomposition

The Pauli decomposition is shown in Fig. 3.

This decomposition makes the following associations between the R, G, B channels of the color image and the polarimetric channels:

- $R = 10\log_{10}\left(|k_{p1}|^2\right)$, where $k_{p1} = \frac{S_{11} - S_{22}}{\sqrt{2}}$;

- $G = 10\log_{10}\left(\left|k_{p2}\right|^2\right)$, where $k_{p2} = \frac{S_{12} + S_{21}}{\sqrt{2}}$;
- $B = 10\log_{10}\left(\left|k_{p3}\right|^2\right)$, where $k_{p3} = \frac{S_{11} + S_{22}}{\sqrt{2}}$;

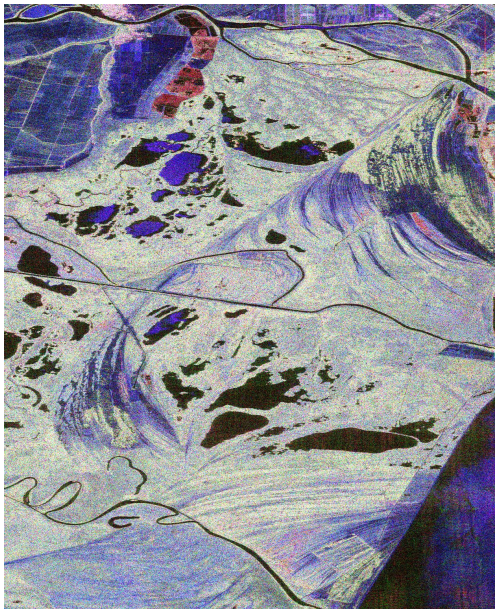

Figure 3: RGB coding of Pauli decomposition

The Pauli decomposition also takes into account the relative phases of the polarimetric channels. It thus allows distinguishing between several elementary mechanisms such as odd- and even-bounce reflexion.

The following interpretations may be attributed to colors:

- blue color generally indicates water or other odd-bounce reflectors, such as plane rough surfaces; this is apparent for the sea and some of the land-locked lakes;
- black color generally indicates still water (also, some land-locked lakes);
- red color generally indicates even-bounce reflexion mechanisms, such as dihedral angles (such as urban environment); one particular region of red color is just below the Chilia channel (in the area of the Chilia Veche town) and another one is on the right side of the image (in the area of C. A. Rosetti and Letea towns);
- green color generally indicates vegetation and this is significantly strong in the middle area of the image (its amplitude is comparable to those of red and blue components, giving the white color).

4. ADVANCED POLARIMETRIC DECOMPOSITIONS

4.1. H/α/A decomposition

The H/α/A decomposition is based on the eigenanalysis of the coherency matrix (the covariance matrix of the Pauli decomposition) of the PolSAR image.

Based on the eigendecomposition of the coherency matrix:

$$\mathbf{T}_3 = \mathbf{U}_3 \mathbf{\Sigma}_3 \mathbf{U}_3^{-1}$$

where

$$\mathbf{\Sigma}_3 = \begin{bmatrix} \lambda_1 & 0 & 0 \\ 0 & \lambda_2 & 0 \\ 0 & 0 & \lambda_3 \end{bmatrix}$$

with

$$\infty > \lambda_1 > \lambda_2 > \lambda_3 > 0$$

and

$$\mathbf{U}_3 = \left[\mathbf{u}_1 \ \mathbf{u}_2 \ \mathbf{u}_3\right]$$

with the parameterizations

$$\mathbf{u}_i = \left[\cos\alpha_i \ \sin\alpha_i \cos\beta_i e^{j\delta_i} \ \sin\alpha_i \cos\beta_i e^{j\gamma_i}\right]^T,$$

the computed quantities are:

- the entropy (H): represents the predictability of the scatterer structure;
- the anisotropy (A): represents the relative weight of the secondary scattering mechanisms;
- the angle (α): can be interpreted for a symmetrical target as the target scattering type parameter and characterizes the mean scattering type mechanism.

The mathematical relations are below:

$$H = -\sum_{i=1}^{3} p_i \log_3(p_i) \qquad p_i = \frac{\lambda_i}{\sum_{k=1}^{3} \lambda_k}$$

$$A = \frac{\lambda_2 - \lambda_3}{\lambda_2 + \lambda_3} \qquad \alpha = \sum_{i=1}^{3} p_i \alpha_i$$

The entropy and the anisotropy of the considered image are depicted in Fig. 4.

From these images, it appears that:

- a significant portion of the image exhibit high entropy and low anisotropy; this show that no dominant scatterer is present and that all the involved scattering mechanisms are of comparable intensity: this is a characteristic for vegetation; the low anisotropy also gives a hint about the structure of the vegetation: it shows that the vegetation consists mainly of numerous very thin cylinders, with various orientations;

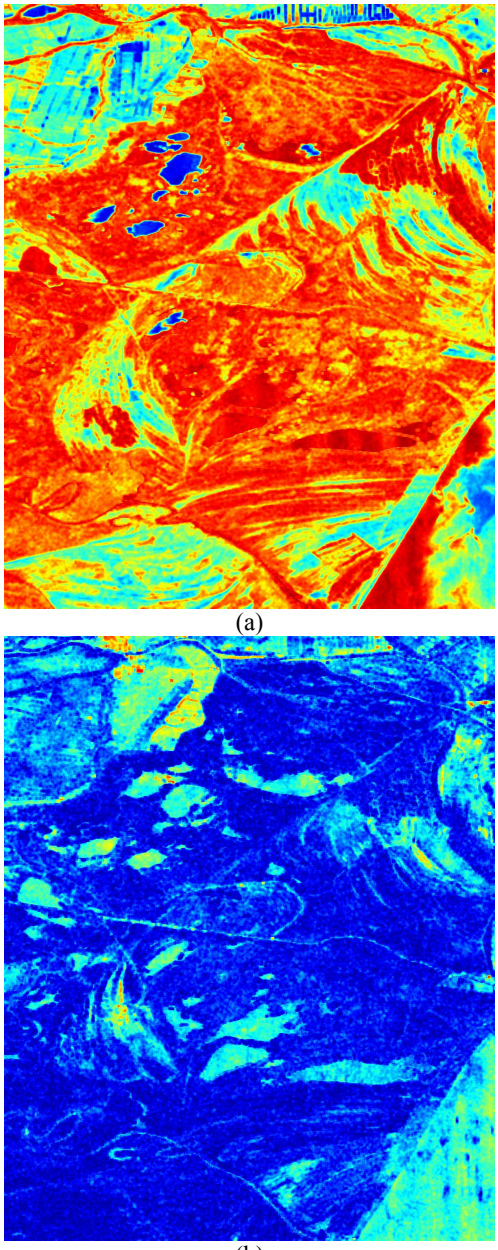

(a)

(b)

Figure 4: Entropy (a) and anisotropy (b) obtained through the H/α/A decomposition

- the sea water exhibits various level of entropy, coupled with moderate-to-high levels of anisotropy; generally, low-level entropy indicate still water, while higher entropy levels indicate rougher water surface; positiveness of the anisotropy show that water reflection does not significantly change the polarization of the incoming wave;
- the urban areas (the towns mentioned above) generally exhibit lower entropy (and, indeed, they are mainly composed of dihedral and trihedral reflectors) with little (anisotropy is moderate-to-high), if any, vegetation.

Based of the values of H and α, a standard classification [3] may be drawn: this is represented in color codes, in Fig. 5.

The color codes are as follows:

- (1) represents either water bodies (at longer wavelengths), either small roughness surfaces;
- (2) (3) (4) represent various vegetation types, also some surfaces with various roughness (may be water, too);
- (5) represents forests or urban areas;
- (6) represents isolated buildings or strong corner reflectors (also a manifestation of man-made constructions).

It may be seen that the above color-coding gives pertinent information about the analyzed landscape.

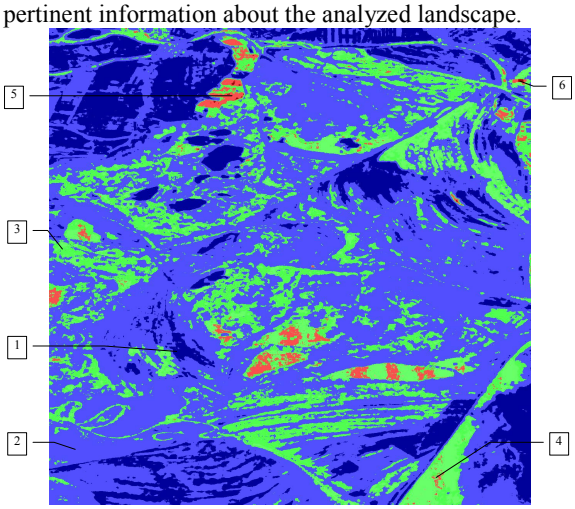

Figure 5: H/α classification

4.2. TSVM decomposition

The TSVM (Target Scattering Vector Model) decomposition is an alternative model for physical characterization of scattering surfaces in PolSAR imaging [4]. It may be applied for both mono-static (where reciprocity condition, i.e. equality of cross-polarization channels, is assumed) and bi-static (where reciprocity condition is unmet) configurations [5].

Since the reciprocity condition is not fully satisfied for the data considered in this report, the bi-static (non-reciprocal) version has been used. The measurable parameters values are illustrated in the following figures. All quantities have been derived from the main scattering mechanism (the first principal vector of the coherency matrix).

The TSVM decomposition rises from the parameterization of the coherent Pauli vectors:

$$\mathbf{k}_p = e^{j\Phi_s} \cdot \begin{bmatrix} 1 & 0 & 0 & 0 \\ 0 & \cos(\theta_R+\theta_E) & -\sin(\theta_R+\theta_E) & 0 \\ 0 & \sin(\theta_R+\theta_E) & \cos(\theta_R+\theta_E) & 0 \\ 0 & 0 & 0 & 1 \end{bmatrix}$$

$$\cdot \begin{bmatrix} \cos(\theta_R-\theta_E) & 0 & 0 & -\sin(\theta_R-\theta_E) \\ 0 & 1 & 0 & 0 \\ 0 & 0 & 1 & 0 \\ -j\sin(\theta_R-\theta_E) & 0 & 0 & -j\sin(\theta_R-\theta_E) \end{bmatrix} \cdot \mathbf{k}_p^{roll-inv}$$

where the first two factors are rotation matrices and are discarded, the useful information being the so-called roll-invariant target vector:

$$\mathbf{k}_p^{roll-inv} = \mu \begin{bmatrix} \cos\alpha_s \cos(\tau_R+\tau_E) \\ \sin\alpha_s e^{j\Phi_{\alpha_s}} \cos(\tau_R-\tau_E) \\ -j\cos\alpha_s \sin(\tau_R+\tau_E) \\ j\sin\alpha_s e^{j\Phi_{\alpha_s}} \sin(\tau_E-\tau_R) \end{bmatrix}$$

$$= \mu \begin{bmatrix} \cos\alpha_s \cos(\tau_1) \\ \sin\alpha_s e^{j\Phi_{\alpha_s}} \cos(\tau_2) \\ -j\cos\alpha_s \sin(\tau_1) \\ j\sin\alpha_s e^{j\Phi_{\alpha_s}} \sin(\tau_2) \end{bmatrix}$$

Meaningful values for the parameters are obtained if parameterization concerns eigenvectors of the coherency matrix instead of coherent Pauli vectors. Generally, the TSVM decomposition refers to this latter approach.

The bi-static angle (α_{s_1}) is depicted in Fig. 6. It characterizes the scattering type mechanism of the dominant scatterer.

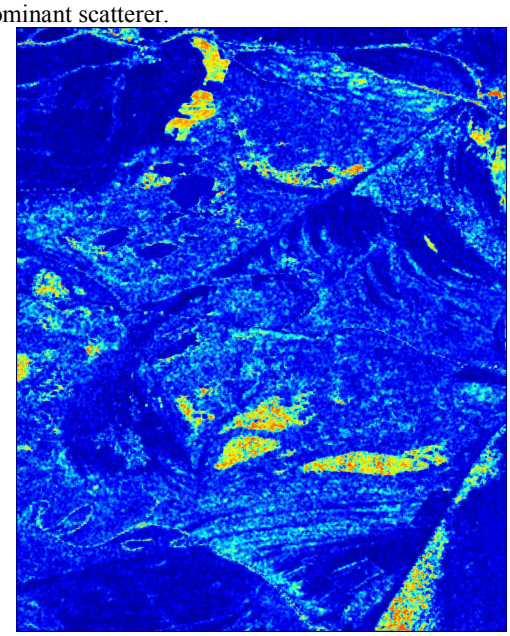

Figure 6: Angle α_{s_1} issued from the TSVM decomposition

Another quantity is $\Phi_{\alpha_{s_1}}$, which has been shown to be sensible to humidity. Its values are depicted in Fig. 7, along with the associated probability ($P_{\Phi_{\alpha_{s_1}}}$, interpretable as a coherency/confidence degree for the associated $\Phi_{\alpha_{s_1}}$ values).

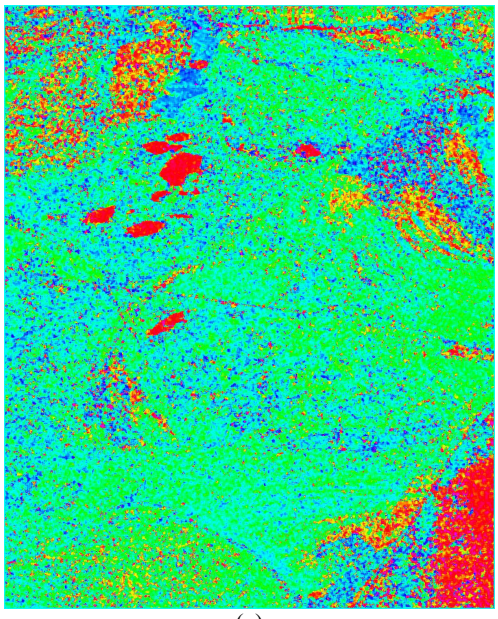

(a)

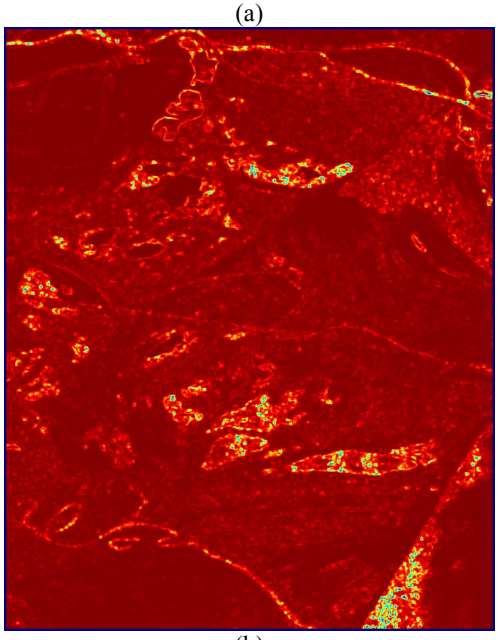

(b)

Figure 7: Parameters $\Phi_{\alpha_{s_1}}$ (a) and $P_{\Phi_{\alpha_{s_1}}}$ (b), issued from the TSVM decomposition

Unfortunately, interpretation of the TSVM parameters is quite difficult and not straightforward, especially for single images (because there is no direct

relation between parameter values and scattering mechanisms). However, comparisons of the associated values between two pair-images may give valuable insight, since differences may be used to track changes between images. Also, a thematic map of the surveyed area may help putting parameter values in correspondence with types of scattering surfaces.

5. STATISTICAL SEGMENTATION

Since the various regions of the PolSAR image have different statistical laws, it is possible to group those regions based on their similarity, thus obtaining an unsupervised classification [6].

The criterion [7] used in the hierarchical segmentation algorithm is based on the log-likelihood function. The algorithm merges the two adjacent segments Si and Sj which minimizes the loss of the likelihood of the partition [8]. The stepwise criterion can be expressed as:

$$SC_{i,j} = GMLL(S_i) + GMLL(S_j) - GMLL(S_i \cup S_j)$$

where $GMLL(S)$ is the generalized maximum log-likelihood function for the segment S (i.e. computed over the pixels belonging to segment S).

The *GMLL* function is computed as follows:

- a parametric probability distribution is assumed for the random data of which pixels in S are considered to be independent realizations;
- the parameters of the parametric distribution are then estimated from those realizations (i.e. the totality of pixels in S) in the maximum likelihood sense;
- the log-likelihood of S is then computed w.r.t. this probability distribution (whose parameters were just computed above), i.e. the log-likelihoods of each individual pixel are summed up;
- the result is the maximal log-likelihood that S may have w.r.t. any among the parametric distribution and is designed as $GMLL(S)$.

The number of segments in the final partition will vary according to the desired detail level.

For example, the partition depicted in Fig. 8 (50 segments) shows several identifiable areas (see legend):

- 1. strong isolated reflector;
- 2. water bodies;
- 3. urban areas;
- 4. sea water with different properties;
- 5. (presumably) dry vegetation or soil;
- 6. (presumably) wet vegetation or soil.

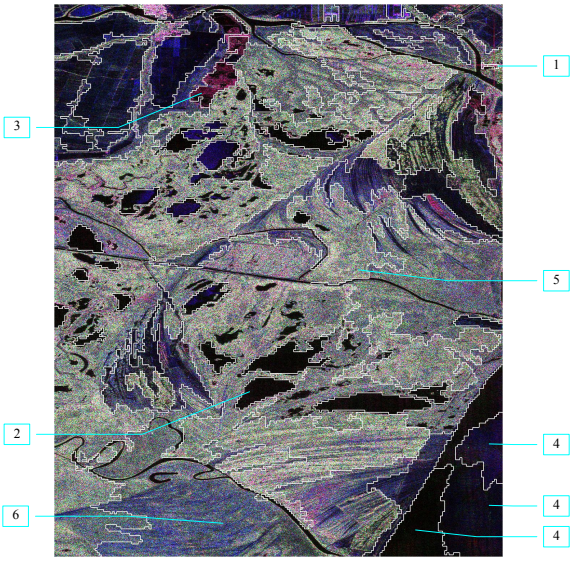

Figure 8: Hierarchical segmentation (50 segments)

It should be noted that the retrieved segments are only groups of similarly statistically distributed pixels (statistics of both texture and speckle are jointly considered here, although it is possible to treat them separately). More refined classification may be achieved through further analyzing the physical properties of those identified segments, for example using the coherency matrix and the subsequently derived H/α/A decomposition. Previously grouping PolSAR pixels in statistically similar regions helps to a more robust estimation of the coherency matrix, since the (sample) averaging is made over a stationary area (in the statistical sense).

Depending on the initial grid partitioning and of the segmentation method performances, segmentation is more or less ideal. However, it may be used as input in human-based post-processing.

6. INTERPRETATION

In Fig. 9a, the optical image provided by the Landsat image system is shown, deformed so that the one-to-one pixel correspondence with PolSAR images shown in this document is ensured. This serves for quick visual comparison.

Also, in Fig. 9b, another version of the Pauli decomposition image is shown. Quick comparison between the two, optical and PolSAR images is thus possible.

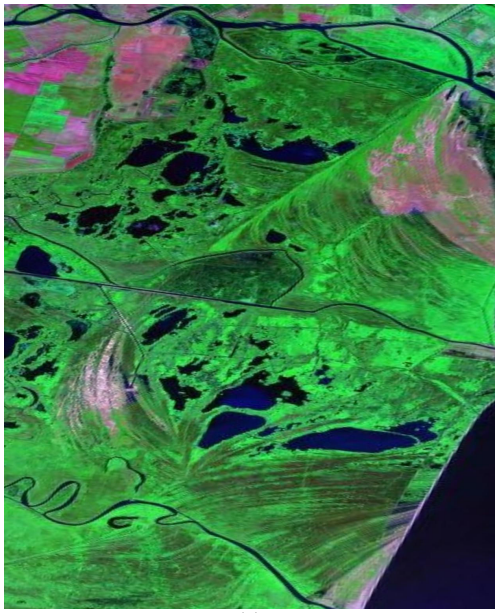

(a)

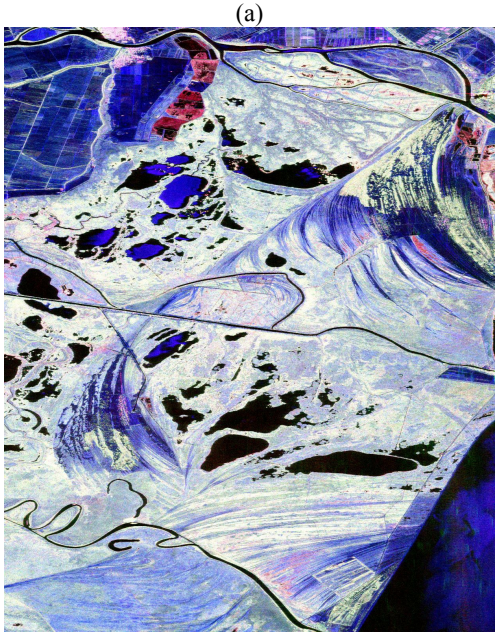

(b)

Figure 9: Optic image (a) and Pauli decomposition of the PolSAR data (b), not rectified versions

Geographically-rectified equivalent optical and radar images are shown in Fig. 10.

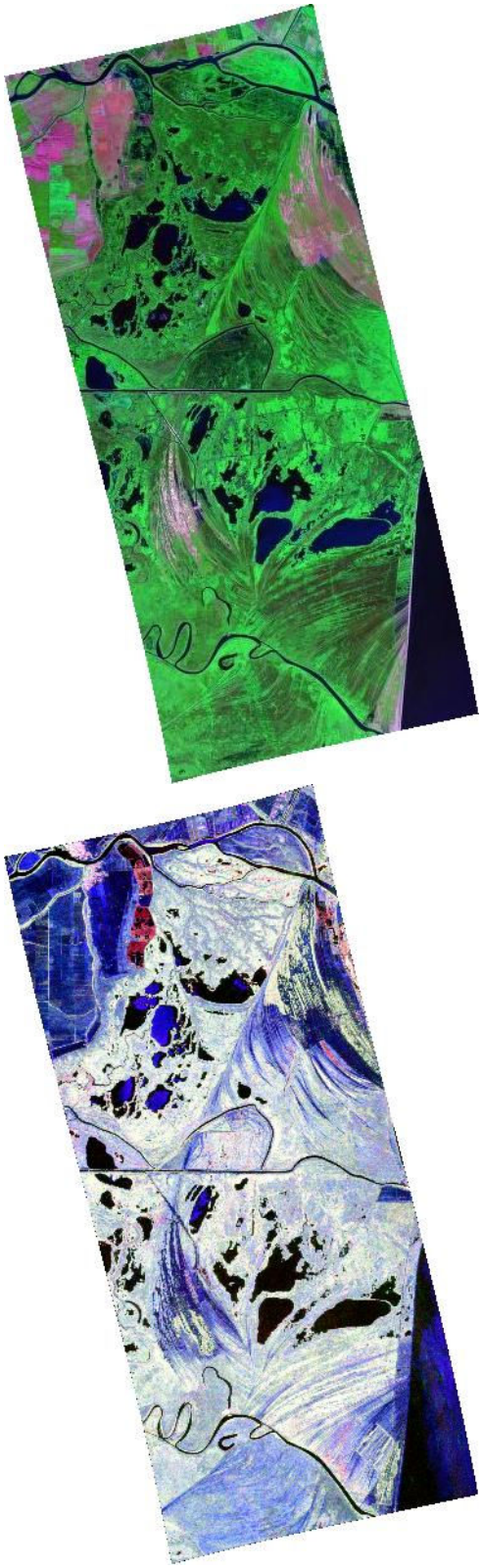

Figure 10: Optic image (top) and Pauli decomposition of the PolSAR data (bottom), rectified versions

Several landscape elements are easily identifiable on the radar image, as shown in Fig. 11.

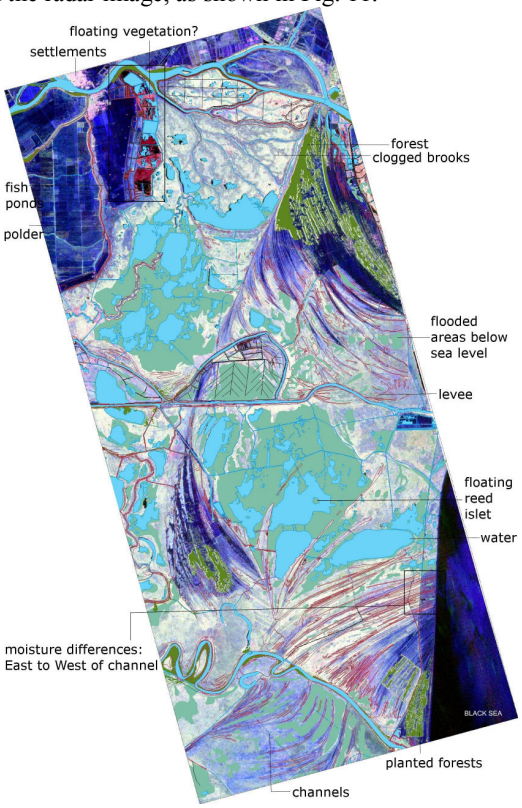

Figure 11: Landscape elements identified on the rectified image

7. CONCLUSIONS

Several methods for exploiting PolSAR data have been presented in this report. Generally, results show exploitable potential for surface characterization.

Perspectives include obtaining interferometric map from two PolSAR images of the same region.

8. ACKNOWLEDGMENTS

The paper uses data provided by the European Space Agency (ESA Category 1 Project Id 7331). This work has been supported by the Advanced Studies and Research Center and the French ANR EFIDIR project.

9. REFERENCES

[1] G. Vasile, J.-P. Ovarlez, F. Pascal, C. Tison, "*Coherency matrix estimation of heterogeneous clutter in high-resolution polarimetric SAR images*", IEEE Transactions on Geoscience and Remote Sensing, vol. 48, No. 4, pp. 1809-1826, 2010.

[2] M. Shimada, "*Advance land-observation satellite (ALOS) and its follow-on satellite, ALOS-2*", ESA SP-668, PolInSAR 2009, Frascati, Italy, 2009, 4 pages.

[3] S. Cloude and E. Pottier, "*An Entropy Based Classification Scheme for Land Applications of Polarimetric SAR*", IEEE Transactions on Geoscience and Remote Sensing, vol. 35, no. 1, pp. 68–78, 1997.

[4] R. Touzi, "*Target Scattering Decomposition in Terms of Roll-Invariant Target Parameters*", IEEE Transactions on Geoscience and Remote Sensing, vol. 45, no. 1, pp. 73–84, January 2007.

[5] L. Bombrun, "*Extension of the Target Scattering Vector Model to the bistatic case*", IEEE International Geoscience and Remote Sensing Symposium, Honolulu, Hawaii, USA, 4 pages, 2010.

[6] J.-M. Beaulieu and R. Touzi, "*Segmentation of Textured Polarimetric SAR Scenes by Likelihood Approximation*" IEEE Transactions on Geoscience and Remote Sensing, vol. 42, no. 10, pp. 2063–2072, 0ctober 2004.

[7] L. Bombrun, J.-M. Beaulieu, G. Vasile, J.-P. Ovarlez, F. Pascal, and M. Gay, "*Hierarchical Segmentation of Polarimetric SAR Images using Heteroge-neous Clutter Models*" in Geoscience and Remote Sensing, IGARSS '09, Cape Town, South Africa, 2009.

[8] L. Bombrun, G. Vasile, M. Gay, F.-C. Totir, "*Hierarchical segmentation of polarimetric SAR images using heterogeneous clutter models"*, IEEE Transactions on Geoscience and Remote Sensing, 2010, to appear.